Studies of Vortex Interference Associated with Missile Configurations

Daniel J. Lesieutre[1] and Omar Quijano[2]
Nielsen Engineering & Research, Inc., Santa Clara, CA, 95054

Studies of vortex-induced aerodynamic nonlinearities associated with body and fin vortices for missile configurations have been performed. As part of this effort, the vortex and fin modeling methodologies in the engineering-level and intermediate-level aerodynamic predictions codes *MISL3* and *MISDL* have been reviewed and improved. The ability of the methods to predict detailed fin loads in the presence of external vortices is demonstrated. Both codes have been used extensively to predict missile performance including canard/wing vortex induced effects on tail fins. These effects often manifest themselves in pitching moments and most dramatically in induced rolling moments on tail fins which counter, and often times reverse, the direct roll control of canard fins. Both codes have shown the capability to capture these vortex-induced phenomena. For validation purposes, the methods were compared to detailed vortex-fin interaction studies, performed at Sandia National Laboratories, which measured fin loads influenced by a vortex generated by an upstream fin.

Nomenclature

AR	=	aspect ratio (two fins joined at root)
C_l	=	rolling moment/$q_\infty S_R l_R$
C_m	=	pitching moment/ $q_\infty S_R l_R$; positive nose up
C_N	=	normal force/ $q_\infty S_R$
C_{NF}	=	fin normal force/ $q_\infty S_R$
D	=	body diameter, maximum
L	=	body length
l_R, L_{REF}	=	reference length
q_∞	=	freestream dynamic pressure
S_R, S_{REF}	=	reference area
x_{CP}	=	fin chordwise center of pressure, or overall configuration axial center of pressure
y_{CP}	=	fin spanwise center of pressure
x_{HL}	=	fin hinge line loaction
x_{MC}	=	moment center
α	=	angle of attack, deg
δ	=	fin deflection angle or angle of attack for fin alone, deg
λ	=	fin taper ratio
φ	=	roll angle, deg

I. Introduction

A study was performed to further assess vortex and fin modeling methodologies in the engineering-level and intermediate-level aerodynamic prediction codes *MISL3*[1-3] and *MISDL*[1,2,4,5], respectively. Details of the vortex modeling and tracking methodology employed are described by Mendenhall.[6] Results include both overall aerodynamic characteristics of configurations with upstream vortices affecting downstream fin sets, and the ability of the methods to predict detailed fins loads in the presence of external vortices.

The *MISL3* and *MISDL* codes have been used extensively to predict missile performance including canard/wing vortex induced effects on tail fins. These effects are seen most dramatically in induced rolling moments on tail fins which counter, and often times reverse, the direct roll control of canard fins. Both codes have demonstrated the

---

[1] Senior Research Engineer, 2700 Augustine Dr, Suite 200, Senior Member.
[2] Research Engineer, 2700 Augustine Dr, Suite 200, Member.

capability to capture this roll-reversal phenomena as well as other induced effects. Ref. 1 details vortex induced nonlinear aerodynamic characteristics, both longitudinal and lateral-directional, of missiles employing tandem-control surfaces[7] (combined canard and tail deflections) and canard control missiles with fixed and free-to-rotate tail fins.[8,9] The study of McDaniel[10] is a comprehensive investigation of the effect of tail fin properties on the induced roll characteristics of a canard control missile and provides great insight into canard vortex tail interactions. Experimental data of Blair[11] and the *MISL3* code were used in the study.

The current investigation includes additional analyses of complete missile configurations, and a detailed study of fin forces and moments in the presence of external vortices. The vortex-fin interaction studies of Beresh,[12] provide detailed fin loads including induced effects from a vortex generated by an upstream fin for different deflection angles. These data are used for further validation. The experimental results include fin normal force, bending moment, and hinge moments. In addition, detailed PIV flow fields were measured.

II. Technical Description

The benefit of engineering- and intermediate-level aerodynamic prediction methods is the computational efficiency needed for initial design studies, trade studies, and generation of large simulation databases. It is critical for missile analysis and design tools to include important nonlinear effects associated with large Mach number ranges and high angles of attack. Both *MISL3* and *MISDL* model these nonlinearities and can analyze many flow conditions quickly to aid the engineer in the preliminary design stage to estimate loads for flight simulations and for structural analysis. Moreover, these tools help the engineer prepare for more costly CFD runs and wind-tunnel tests. The following sections summarize the methodologies in the two prediction methods and recent enhancements.

A. Description of *MISL3*

The engineering-level aerodynamic prediction code *MISL3*[1-3] has been developed for aerodynamic performance prediction and for preliminary design of conventional missiles. The method uses the Triservice fin-on-body force and moment data base.[13,14] The prediction methodology employed covers a Mach number range from 0.5 to 5.0, fin aspect ratios from 0.25 to 10.0, angles of attack to 90°, arbitrary roll angles, and deflection angles from -40° to 40°. The method uses the equivalent angle of attack concept, which includes the effects of vorticity and geometric scaling. Ref. 3 provides more details regarding the methodology employed and presents comparisons to experimental data for a wide variety of configurations. Fig. 1 depicts the fin and body vortex modeling for a canard-tail configuration.
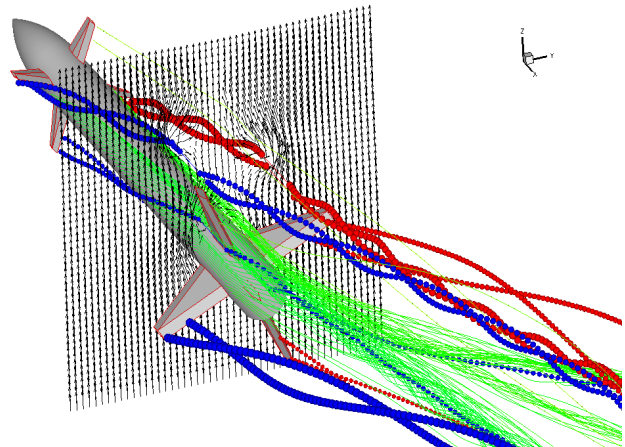

Figure 1. MISL3 vortex modeling.

B. Description of *MISDL*

The intermediate-level aerodynamic prediction code *MISDL*[1,2,4,5] is based on panel methods and classical singularity methods enhanced with models for nonlinear vortical effects. It predicts longitudinal and lateral-directional aerodynamic characteristics, including nonlinear Mach number, body and fin vortex wake effects. *MISDL* can model noncircular body configurations and configurations with unconventional fin shapes. The body of the missile is modeled using

Figure 2. MISDL calculation procedure and paneling.

conformal mapping (if noncircular), and either subsonic or supersonic sources/sinks and doublets for volume and angle of attack effects, respectively. The fin sections are modeled by a horseshoe-vortex panel method for subsonic flow, and by constant pressure panels for supersonic flow. Up to three fin sections can be modeled, and nonlinear fin and body vortices are included. The *VTXCHN* methodology, a vortex-cloud method,[6] is used to represent body shed vorticity. The overall calculation proceeds as follows: 1) the forebody loads are computed, including the effects of body vortex shedding and tracking, 2) loads within the forward fin set are calculated, including the effects of forebody vorticity, 3)
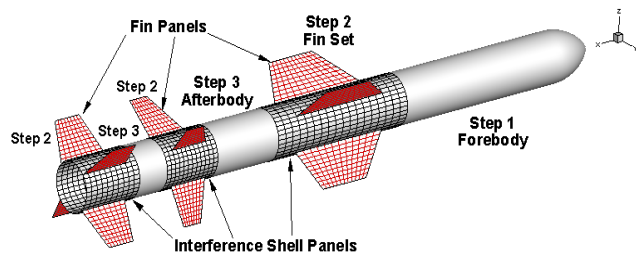
the vorticity shed from the forebody and the forward fin set is included as an initial condition in the *VTXCHN* module which tracks and models additional vortices shed from the afterbody, and 4) if second or third fin sets are present, steps 2 and 3 are repeated. A schematic of the calculation steps and paneling layouts is shown in Fig. 2.

Recent enhancements in *MISDL* have included additional options for specification of shed vortex properties (core size), improved deflected fin shed vorticity, better modeling of lifting surfaces with flaps, increasing the number of circumferential body panels within a fin section to better capture mutual fin-body carryover forces, and the option to extend the fin section body panels both forward and aft of the fin leading- and trailing-edges to increase the fidelity of fin-body loading carryover.

The range of parameters of the *MISDL* code includes Mach numbers from 0.0 to 3.0 with a modified shock-expansion capability to higher supersonic speeds, angles of attack up to 20°, arbitrary roll angles, and rotational rate effects. For bodies alone, the angle of attack range limit exceeds 40°. Fins can have arbitrary planform shape and spanwise dihedral, including wrap-around and folded fins.[4] An empirical stall model is included for fins at high angles of attack. A version of *MISDL* employing an optimizer has also previously been used to design unconventional fin planforms for several design objectives, such as minimization of fin hinge moments and maximization of normal force.[5]

Fig. 3 is an illustrative prediction for a circular ogive-cylinder body at high angle of attack. The predicted pressure distribution and body shed vortex wake are shown. The body vortex shedding and tracking of individual vortices of the vortex "cloud" are colored in proportion to their individual strengths. The crossflow velocity vectors and the low pressure region below the vortices on the lee-side of the body show the strong influence of the body shed vorticity on both the local flow field and surface pressures.
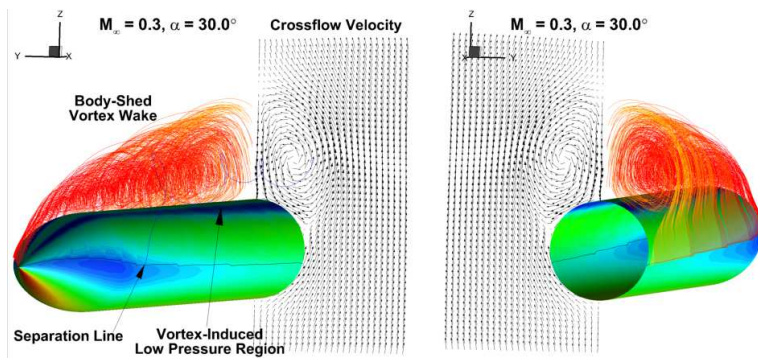

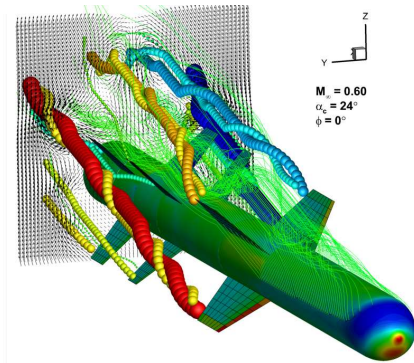**Figure 3. Example prediction of body-alone at high angle of attack.**

Figure 4. Three fin-set prediction.

Fig. 4 shows predicted results for a three fin-section missile at high angle of attack. The predicted pressure coefficient is plotted on the body surface, while the loading pressure, ΔC_P, is shown for the fins. The location of vortices is indicated by spherical symbols which are colored and sized in proportion to the vortex strength. The details of the flow fields predicted are useful for understanding the character and interference effects of the flow at high angles of attack.

III. Results

This section presents predicted and measured results for several configurations which include strong vortex induced effects. The first set of results compares *MISL3* and *MISDL* predictions with the detailed fin vortex interaction study of Beresh.[12] This is an important study because it measured fin loads in the presence of a well-defined vortex shed from an upstream fin. The measurement of fin forces and moments and PIV flow fields aids the analysis. In addition to the detailed fin loads study, the tandem control and fixed- and rolling-tail configurations from Ref. 1 are revisited because of recent code enhancements and the investigation of additional data contained in Refs. 7-9.

A. Fin Interaction with a Trailing Vortex

The *MISL3* and *MISDL* methods were employed to simulate the experimental setup in Ref. 12 which included upstream and downstream fins mounted on the wall of the Sandia wind tunnel. The experimental setup is shown in Fig. 5. Both fins could be deflected, and the upstream fin was used to generate vorticity to influence the downstream fin. To model this fin-on-wall setup with *MISL3*, the configuration was approximated by placing the fins on a very large diameter body. This is the same approach
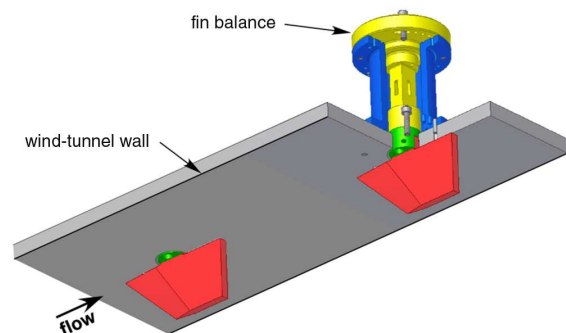

Figure 5. Sandia fin vortex interference setup.

used in Ref. 12 for obtaining Missile DATCOM results. Fig. 6 compares the predicted and measured fin loads without the upstream fin or vortex present. The figure shows the effect of Mach number on (from left to right) the fin normal force, bending moment, and hinge moment as a function of fin deflection angle (angle of attack). In Fig. 6, the symbols represent the experimental data, while the lines represent *MISL3* predictions. The normal force and bending moment are predicted well, including the small Mach number variation trend. The hinge moment is not predicted well, so the fin center of pressure was investigated. The spanwise and chordwise center of pressures, computed using the fin force and moments, are shown in Fig. 7. For significant loading (higher angles), the difference between the measured and predicted spanwise and chordwise centers of pressure is less than 5% of the fin span and root chord, respectively. The hinge moment, and thus the axial center of pressure, is the most sensitive parameter and this is discussed in the next section of the paper.
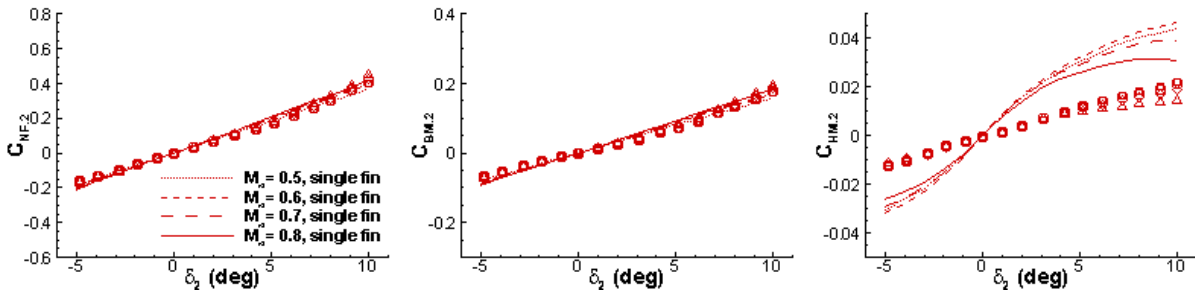

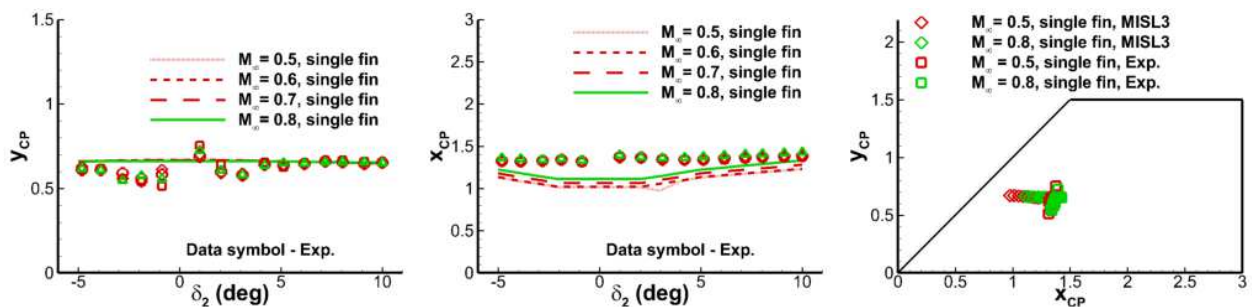**Figure 6. *MISL3* predicted fin-alone loads.**

Figure 7. Measured and *MISL3*-predicted center of pressure (inches).

Fig. 8 depicts the measured and *MISL3*-predicted downstream fin loads as a function of its deflection angle with the upstream fin at deflection angles from -5 to 10 degrees. (Fig. 5 of Beresh[12]). The variation in shed vortex strength with increasing deflection results in flow-induced local angles of attack and modified loads on the downstream fin. The normal force and bending moment, which include the induced effects from the upstream fin vortex, are seen to compare well with the experimental data. Like the single fin results, Fig. 7, the predict hinge moment are larger in magnitude than the experiment. These are addressed in the following section.
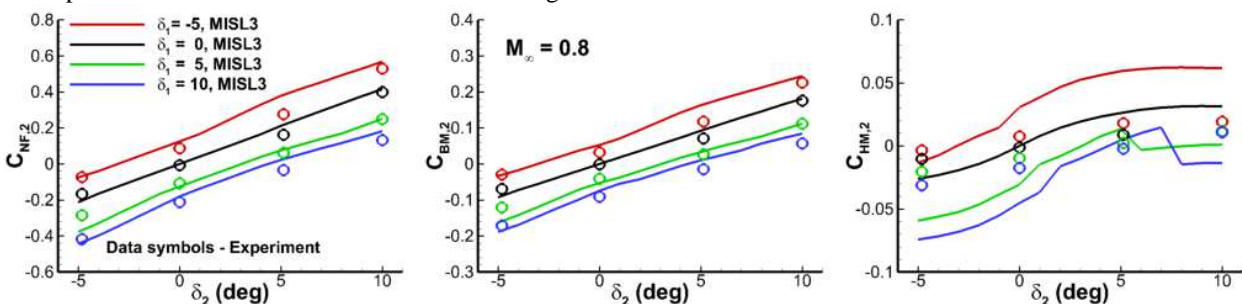

Figure 8. *MISL3* predicted loads with vortex influence from upstream fin, $M_\infty = 0.8$.

With *MISDL*, there are several means to approximate the fin-on-wall setup of the experiment. These include the modeling of a larger diameter body approach, as in *MISL3*, adding to the fins of interest additional large vertical fins which approximate the wall, or alternatively modeling the fins as wings alone (two fins joined at the root chord), which is equivalent to a symmetry plane for inviscid flow. All approaches should be capable of achieving similar results in

principle, but modeling the large diameter body is problematic, due to body paneling resolution issues with respect to the fins. The two other approaches, modeling of the the wall as vertical fins (not shown), and the wing-alone approach, were found to achieve similar results.

Figs. 9 and 10 compare *MISDL*-predicted and measured fin forces, moments, and centers of pressure utilizing the wing-alone approach. The results are similar to the *MISL3* predictions. The normal force and bending moments are predicted well, and the centers of pressure agree with experiment, to within 5% of the span and root chord length. The hinge moments are over predicted, similar to *MISL3*.
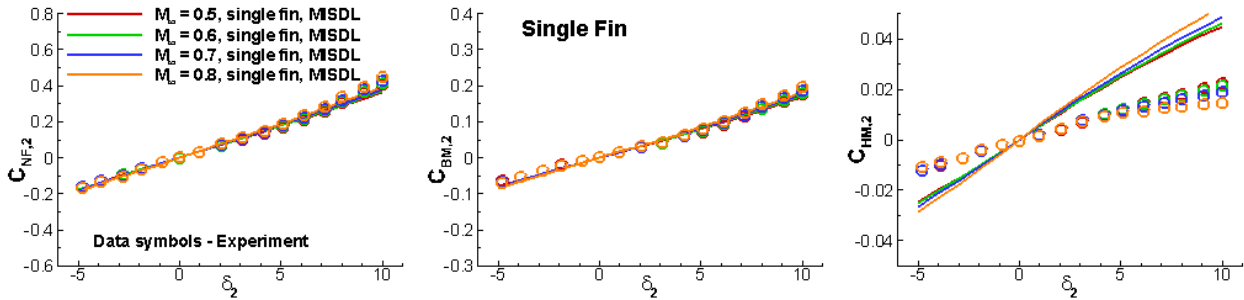

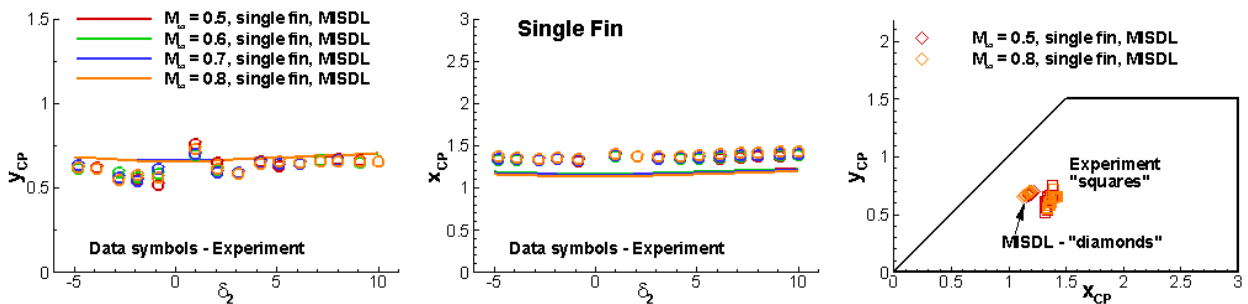
Figure 9. *MISDL*-predicted fin-alone loads.

Figure 10. Measured and *MISDL*-predicted center of pressure (inches).

The measured and *MISDL*-predicted downstream fin loads in the presence of the upstream fin deflected at angles from -5 to 10 degrees are shown in Fig. 11. The *MISDL*-predicted normal force and bending moment, which include the induced effects from the upstream fin vortex, compare well to the experimental data. A detailed discussion of the hinge moments follows in the next section.
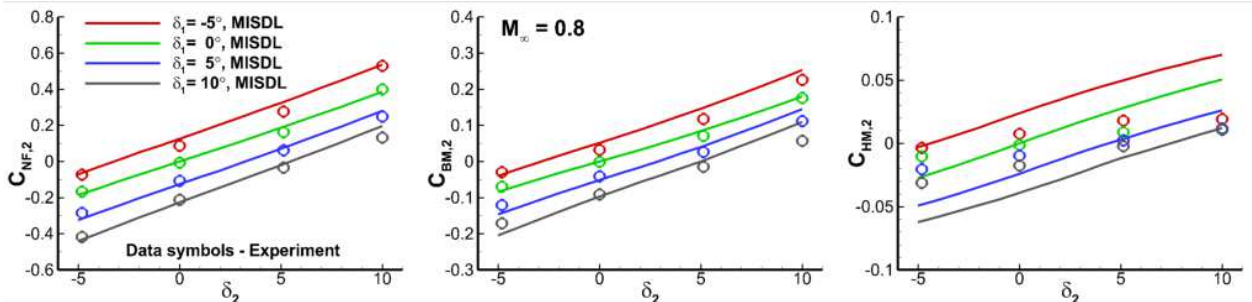

Figure 11. MISDL predicted loads with vortex influence from upstream fin, $M_\infty = 0.8$.

B. Transonic Hinge Moments

The ranges for the predicted hinge moment calculated by *MISL3* and *MISDL* are larger than indicated by the experimental data. This is due to differences in physics between the experiment and the *MISL3* and *MISDL* modeling. In the experiment, the reality is that the flow past the mounting wall and the fin develops a viscous boundary layer. The Triservice fin-on-body database[14] used by *MISL3* includes viscous effects, but they are for a smaller diameter body which curves away from the fins. *MISDL* is an inviscid panel-method based prediction and, thus, does not account for any boundary layer effects.

Another consideration is that for subsonic and transonic flow conditions the hinge moments are sensitive to the fin thickness profiles. A primary difference between the Triservice fins and the Sandia fin is their thickness profile, which

can have a stronger effect on the hinge moment (axial center of pressure) than on either the normal force or the bending moment. The Triservice fins have double-wedge thickness profiles.[14] The Sandia fin has a wedge leading-edge for the first 30% of chord, followed by a constant thickness profile for the remainder of the chord.[12] For the Mach numbers tested (0.5, 0.6, 0.7, and 0.8), the hinge moment is sensitive to the thickness profile. An additional fin-on-splitter plate data set,[15] has a fin with the exact dimensions as the Sandia fin: 3 inch root chord, 1.5 inch tip chord, and 1.5 inch span. Its thickness profile is a modified double wedge (LE wedge, flat section, TE wedge). The geometries of the Sandia,[12] *MISL3* (Triservice – between fins F42 and F52),[1-3,13,14] and NASA fins.[15] are shown in Fig. 12. Fig. 13 compares the experimental results (Triservice is from MISL3 implementation) for fin normal force, bending moment, and hinge moment for all three fins at different deflection angles. The hinge moment is seen to be the parameter that is most sensitive to the fin geometry variations. Note that the Triservice/*MISL3* results shown in Fig. 13 are are not "measured" data from the Triservice database. Instead, in *MISL3*, the Triservice fin-on-body data are processed to correlate fin centers of pressure with fin normal force, etc., and the correlations are used within the equivalent angle of attack methodology to predict loads.
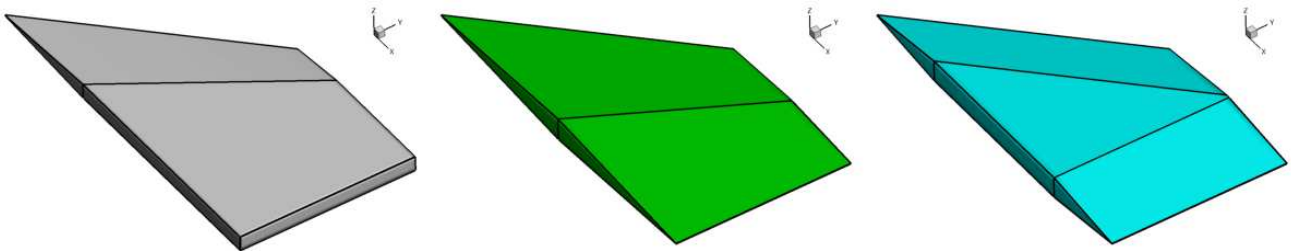

Figure 12. Comparison of fin thickness profiles, Sandia,[12] Triservice,[1-3,13,14] NASA.[15]
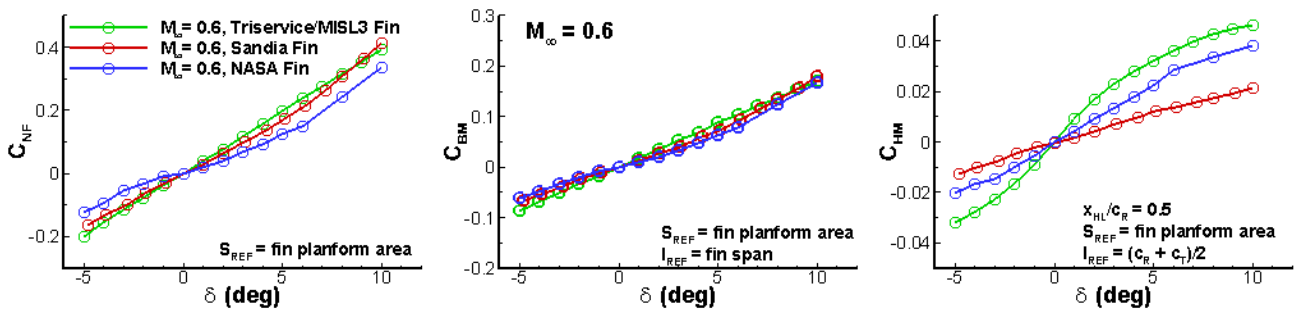

Figure 13. Fin thickness distribution effect on fin loads at $M_\infty = 0.6$.

Fig. 14 depicts the fin spanwise and chordwise centers of pressure for the three fins. The Triservice and NASA fins exhibit centers of pressure forward of the Sandia fin. The computed centers of pressure from the NASA fin data from -3 to 0° angle of attack are sensitive to the small fin normal forces that were measured. Note that the measured data for negative and positive angles of attack are not sysmmetric as would be expected. For this data (NASA -3 to 0°), the computed center of pressure is off the fin.
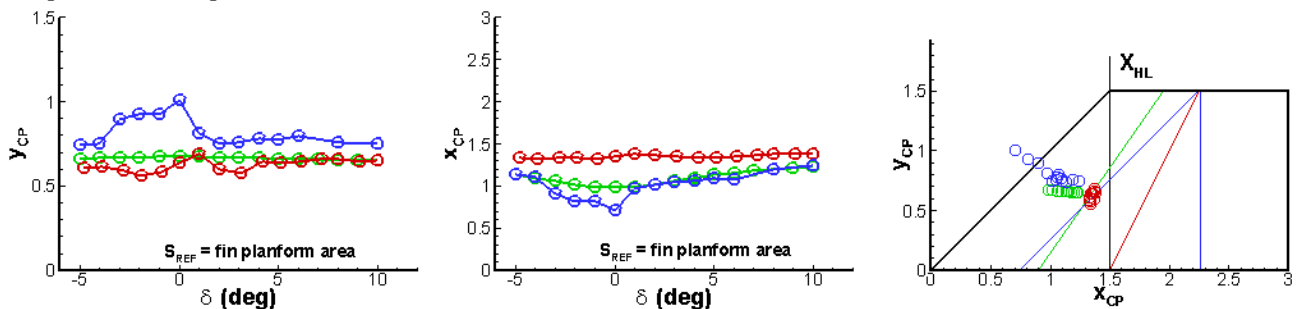

Figure 14. Fin thickness distribution effect on fin center of pressure (inches) at $M_\infty = 0.6$.

The effect of the thickness profile on the hinge moments was also investigated with a preliminary CFD study using the CART3D Euler solver.[16] The three fins in Fig. 12 were meshed, and loads were computed with CART3D after the residuals converge by three orders of magnitude. The results are shown in Fig. 15. Once again, the hinge moment is the

parameter exhibiting the largest amount of variation. Note, however, that the CART3D Euler solutions for the three fins are in fairly close agreement with one another. This suggests that further analysis using a viscous CFD solution may be required to clarify the role of the wind tunnel boundary layer with respect to the observed differences in hinge moments. For subsonic Mach numbers, the force generated by a lifting surface is located forward, toward the leading edge. Thus, a reduction in fin force along the root chord due to the wall boundary layer is consistent with an aft movement of the center of pressure.
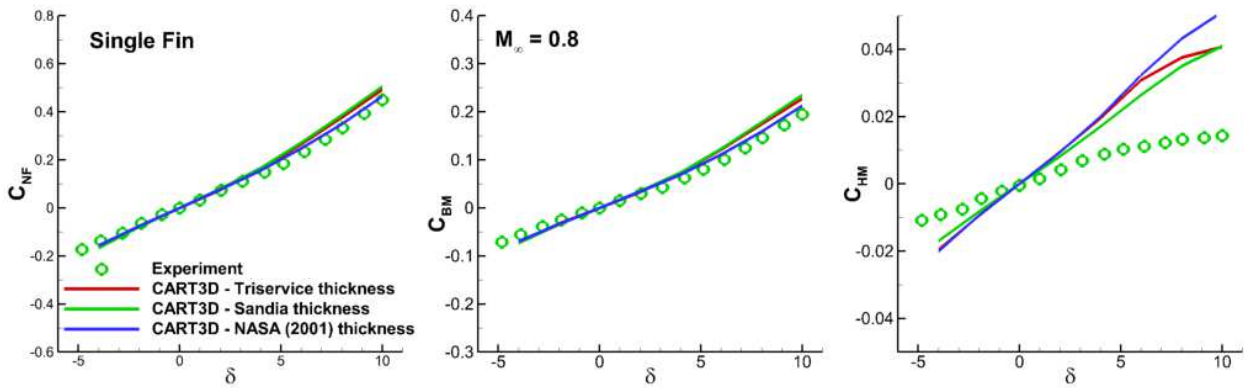

Figure 15. CART3D predicted results for the three fin thickness profiles.

C. Tandem Control Missile Model

The Tandem-Control data presented in this section were obtained from tests conducted in the NASA/LaRC Unitary Plan Wind Tunnel at freestream Mach numbers ranging from 1.75 to 2.86.[1,8] The test objective was to provide an aerodynamic database to study and evaluate tandem control effectiveness. The model consists of a 3-caliber ogive nose followed by a 12-caliber cylinder with cruciform inline canards and aft tail fins. Tests were performed on two models. Both models had the same canard fins, AR = 1.6 and λ = 0.625 (designated C4). Two tail fin geometries were tested: 1) tail fins identical to the canard fins (designated T4), and 2) larger span tail fins (deginated T3). The model shown in Fig. 16 has the larger span tail fins, AR = 2.33 and λ = 0.625. Model aerodynamic forces and moments were measured with an internally mounted six-component strain-gage balance. To assure turbulent flow over the model, all tests were performed with boundary-layer transition strips located on the model nose and near the leading edges of the fins. The test Reynolds number, based on body diameter, was 4.33×10^5.
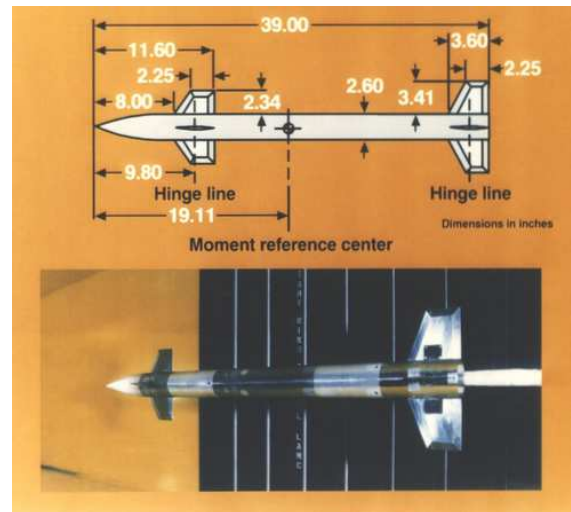

Figure 16. Tandem control wind tunnel model.

Fig. 17 compares the wind-tunnel measurements (indicated by round symbols) to the *MISL3* and *MISDL* predicted aerodynamic characteristics of the B1T4C4 configuration at a roll angle of 45° - the "X" flying configuration. Results are shown for zero canard deflection, $\delta_C = 0°$, and for the canards deflected +5° to produce a positive pitching moment. Comparisons are made of normal force, pitching moment, and center of pressure. The experiment $\varphi = 45°$ condition exhibits several minor nonlinearities in the normal force, which are especially apparent in the pitching moment and computed axial center of pressure (in diameters from moment center). This is due to body and canard vortices interacting with the lower and upper tails fins at different angles of attack. Nonlinear behavior is seen over the whole angle of attack range with more dramatic effects at angles around 0° and in the range from 8-14° The axial center of pressure is predicted to within a body radius over the angle of attack range.
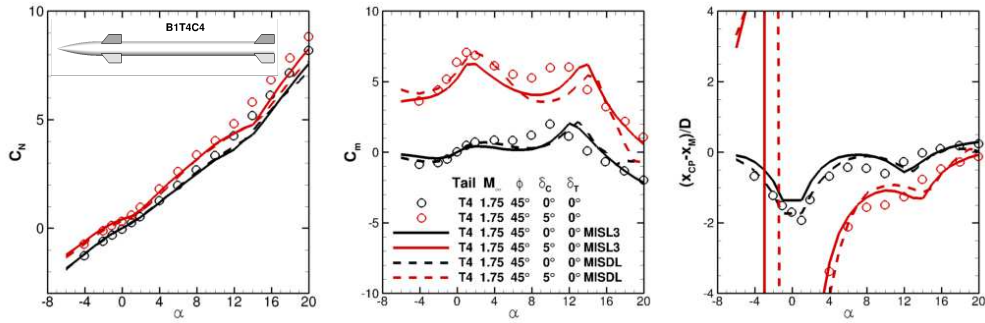
American Institute of Aeronautics and Astronautics

Figure 17. Configuration B1T4C4 normal force, pitching moment, and center of pressure with canard pitch deflections of 0° and +5°, $M_\infty = 1.75$, $\varphi = 45°$.

To better understand the pitching moment characteristics, individual fins loads predicted by *MISL3* and *MISDL* are shown in Fig. 18. *MISL3* results are in the upper graphs and *MISDL* in the lower ones. In addition, the *MISDL*-predicted crossflow velocity fields at the tail leading edge are shown in Fig 19 for angles of attack of 2, 8, and 14 degrees. The two left graphs of Fig. 18 show the predicted canard fins loads. The windward side canards loads indicate fully loaded fins without any vortex influence or fin stall effect; this is as expected. For the leeward side fins, *MISL3* indicates a large unloading effect; by contrast, *MISDL* only shows a slight unloading at the higher angles of attack. *MISL3* uses an empirical forebody vortex model and may includes body flow phenomena contained within the Triservice fin-on-body database. *MISDL* predicts forebody separation and vortex strengths based on the *VTXCHN* approach. The differences are still being examined. The middle set of graphs contains the predicted fin loads for the windward tail fins, and the right graphs of Fig. 18 show the predicted loads on the leeward tail fins. The green curves are the tail fin loads without the canard fins modeled (body-tail), but with body vortex shedding modeled. Both the $\delta_C = 0°$ and $\delta_C = +5°$ results indicate vortex induced loads on the windward tail fins. These effects are evident for angles of attack below 8°. This is also evident in the velocity fields shown in Fig. 19. For $\delta_C = +5°$ and angles of attack below 4° all of the tail fins have a negative normal force (canard vortex induced) which results in enhanced positive nose up pitching moments, as seen in Fig. 17. Above $\alpha = 8°$, the canard shed vortices track upward far enough that the windward fins begin to recover and approach the no-canard results. By comparison, the leeward tail fins are susceptible to induced canard and body shed vortex effects over the whole angle of attack range. At low angles, the leeward canard vortices influence the leeward tails, and, as the angle is increased, body vorticity is shed and the windward canard fin vortices track upwards and impinge on the leeward tails. As previously mentioned, the green curve is the leeward fin load without canard fins (body-tail). For the $\delta_C = 0°$ and $\delta_C = +5°$ results, significant interference is seen over the whole angle of attack range. The largest influence is seen at angles of attack from 12 to 14; this is the range when the strong windward canard vorticies impact the leeward tail fins, as seen in Fig. 19, and as experienced in the configuration pitching moment, Fig. 17.
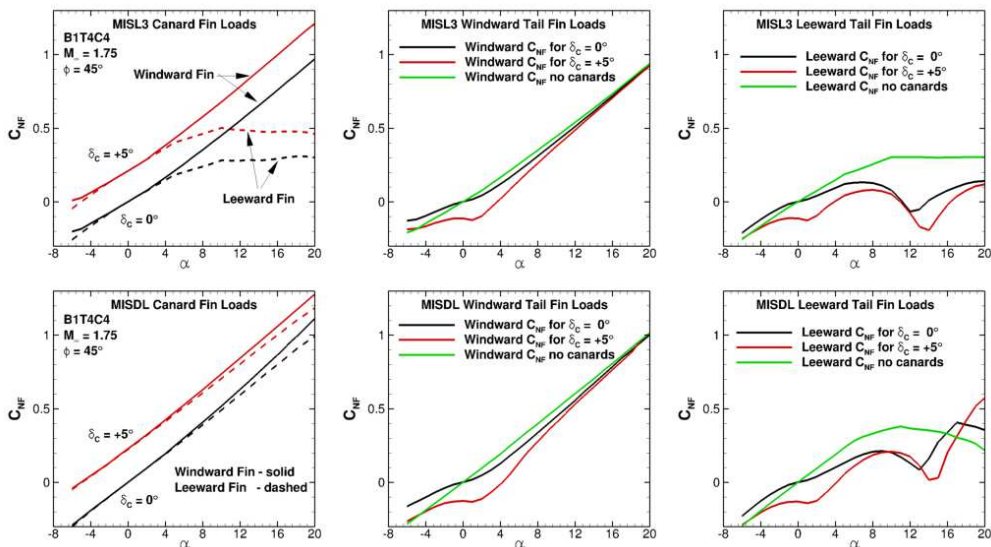

Figure 18. Predicted MISL3 and MISDL fin normal force coefficients, C_{NF}.
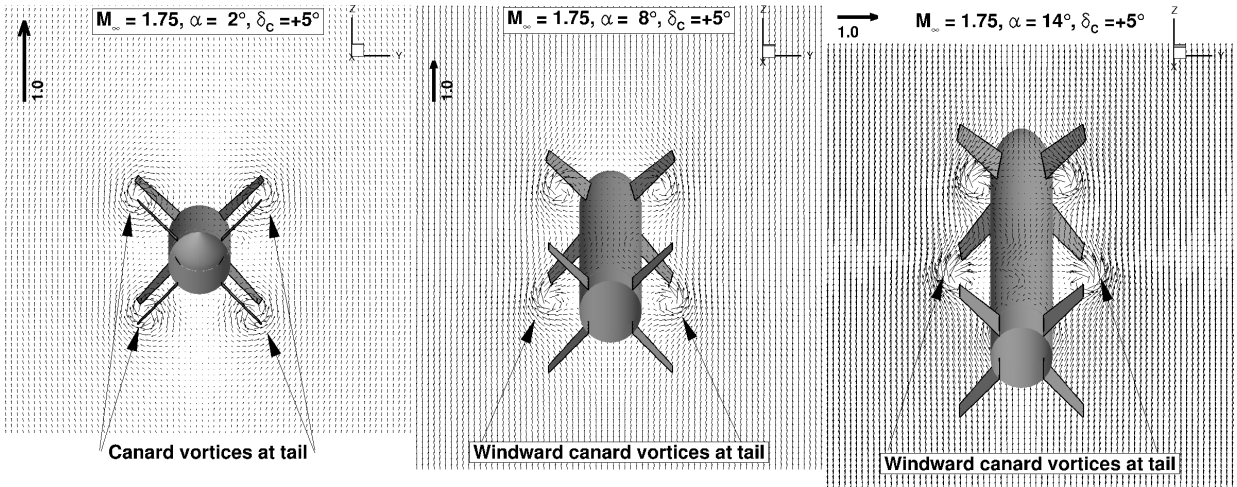
Figure 19. MISDL predicted crossflow velocities at tail fins.

The prediction of combined canard and tail deflections for pitch control are shown in Fig. 20 for the B1T4C4 configuration at roll angles of 0° and 45°. The canards are deflected positive and the tails are deflected negative to produce positive pitching moment. The pitching moment characteristics are different for the two roll angles, and the codes predict the moments and trends well.
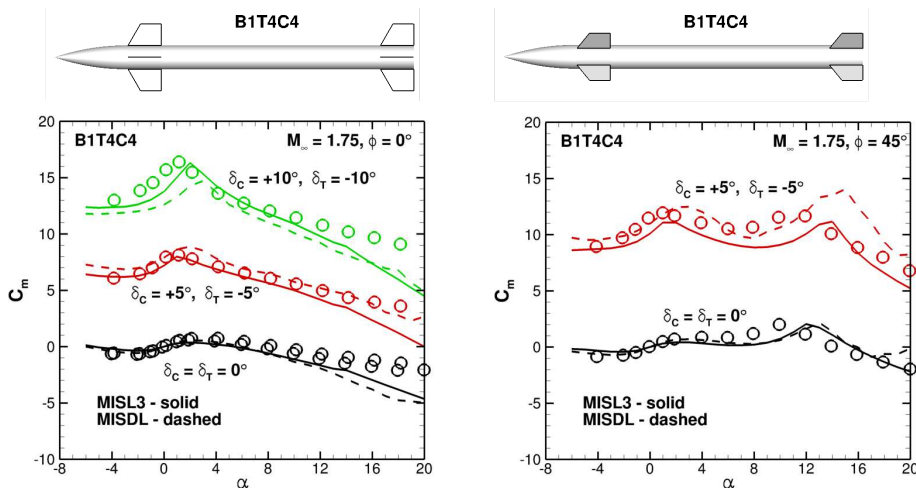

Figure 20. Combined canard/tail deflections to produce pitch, $M_\infty = 1.75$, $\varphi = 0°$ and $45°$.

D. Missile Canard Control and Induced Roll

The *MISL3* and *MISDL* prediction methods have been used to estimate canard vortex tail interactions for a variety of configurations as shown in Refs. 1-3 and 10. The canard tail configuration of Blair[9] illustrates canard-induced roll control effects on tail fins. The wind-tunnel model is shown in Fig. 21. This model was used in Ref. 1 and is shown here to illustrate the prediction the nonlinear induced loads. The model has a 3-caliber tangent-ogive nose and an overall body length of 15 diameters. The test Reynolds number, based on body diameter, was 4.17×10^5.
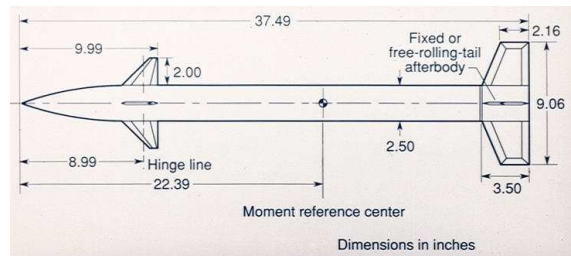

Figure 21 Canard-tail configuration of Ref. 9.

Fig.22 compares measured[9] and predicted rolling moment for a Mach number of 1.7 with the horizontal canards deflected for roll control, $\delta_{ROLL} = -5°$ ($\delta_{ROLL} = (\delta_{C2} - \delta_{C4})/2$). Measured and predicted results are shown for the canards in

the "+" orientation and the tails in the "x" orientation (C+Tx configuration). The measured data for the configuration are also shown with the tail section free to rotate (C+T-free); the tails do not produce a rolling moment except through bearing friction (negligible). It is seen in Fig. 22 that the *MISL3* predicted direct roll control is in very good agreement with the measured C+T-free rolling moment. *MISDL* slightly overpredicts the canard rolling moment. For the C+Tx configuration, the *MISL3* predicted rolling moments agree well with data up to 4° angle of attack and have the correct trends above 4°. *MISDL* predicts the rolling moments very well in magnitude and trend. This type of rolling moment is difficult to predict because it is dominated by the canard and body shed vortices influencing the tail fins. This is the classical induced roll effect seen on canard-controlled missiles. For these configurations, the induced tail fin rolling moment opposes the direct canards control and actually causes the overall rolling moment to oppose the intent of the canard deflection. Above 14°, the *MISL3* and *MISDL* predictions continue their trend and the experiment appears the approach the canard alone rolling moment. As the angle of attack is increased, the canard vortices move away from the tail fins; while the body vorticity remains lower. Ref. 1 includes detailed crossflow velocity plots. If the body shed vorticity is asymmetric, as a result of asynmmetric canard vortices, the tails still experience induce rolling moments. If the canard fins stall resulting in similar loads from the two deflected fins, one would expect nearly symmetric "wakes," and a rolling moment which approaches zero as the angle of attack is increased even further.
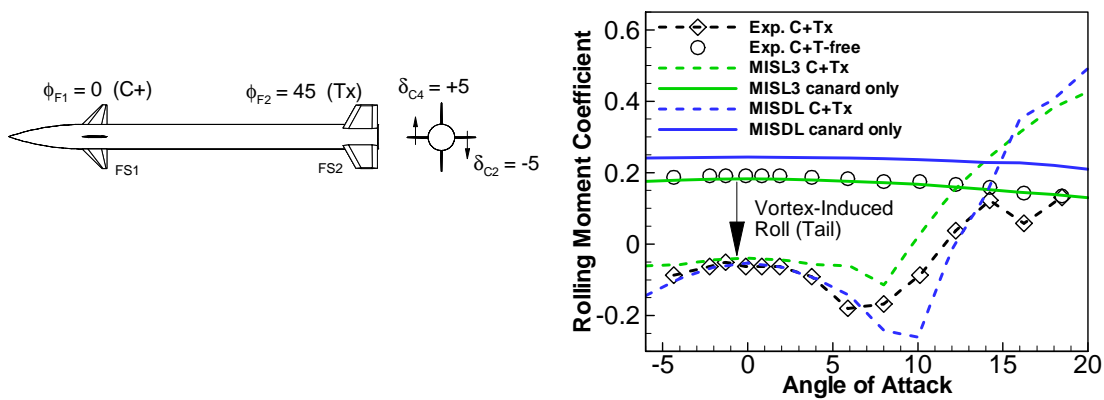

Figure 22 MISL3 and MISDL predicted direct and induced rolling moments.

IV. Conclusion

This paper presents a detailed investigation of the capabilities of engineering- and intermediate-level aerodynamic prediction methods to estimate vortex-induced fin loads. The ability to predict the nonlinear induced effects of an upstream vortex on a downstream fin (normal force , bending moment, and hinge moment) was shown along with CART3D Euler CFD estimates of the fin-alone loadings. In addition, predictions of the nonlinear aerodynamic characteristics of missile configurations with tandem-controls and free-rolling tail sections were investigated. These configurations have eight individual fins which each experience induced effects. Computing pitch-plane and lateral directional aerodynamic characteristics can be challenging for these conditions. In general, the predicted aerodynamic characteristics are in good-to-excellent agreement with the experimental data and, importantly, provide insight into the understanding of the nonlinear aerodynamic characteristics of missile fins and missile configurations.

Acknowledgments

References

[1]Lesieutre, D. J., Love, J. F., and Dillenius, M. F. E., "Prediction of the Nonlinear Aerodynamic Characteristics of Tandem-Control and Rolling-Tail Missiles," AIAA 2002-4511, Aug. 2002.

[2]Dillenius, M. F. E., Lesieutre, D. J., Hegedus, M. C., Perkins, S. C., Jr., Love, J. F., and Lesieutre, T. O., "Engineering-, Intermediate- and High-Level Aerodynamic Prediction Methods and Applications," *Journal of Spacecraft and Rockets*, Vol. 36, No. 5, Sep.-Oct. 1999, pp. 609-620.

[3]Lesieutre, D. J., Love, J. F., Dillenius, M. F. E., and Blair, A. B., Jr., "Recent Applications and Improvements to the Engineering-Level Aerodynamic Prediction Software *MISL3*," AIAA 2002-0275, Jan. 2002.

[4]Lesieutre, D. J., Dillenius, M. F. E., and Gjestvang, J., "Application of MISDL/KDA Aerodynamics Prediction Method to Penguin Missile," AIAA 2002-0277, Jan. 2002.

[5]Lesieutre, D. J., Dillenius, M. F. E., and Lesieutre, T. O, "Multidisciplinary Design Optimization of Missile Configurations and Fin Planforms for Improved Performance," AIAA 98-4890, Sep. 1998.

[6]Mendenhall, M. R., Perkins, S. C., Jr., and Lesieutre, D. J., "Vortex Cloud Model for Body Vortex Shedding and Tracking," *Tactical Missile Aerodynamics: Prediction Methodology*, ed. by M. R. Mendenhall, AIAA, 1992, pp. 225-285.

[7]The Tandem-Control Data taken by A. B. Blair, Jr., NASA Langley Research Center.

[8]Blair, A. B., Jr., "Wind-Tunnel Investigation at Supersonic Speeds of a Remote-Controlled Canard Missile With a Free-Rolling-Tail Brake Torque System," NASA TP 2401, Mar. 1985.

[9]Blair, A. B., Jr., "Supersonic Aerodynamic Characteristics of a Maneuvering Canard-Controlled Missile with Fixed and Free-Rolling Tail Fins," SAE Paper 901993, Oct. 1990.

[10]McDaniels, M. A., Evans, C., and Lesieutre, D. J., "The Effect of Tail Fin Parameters on the Induced Roll of a Canard-Controlled Missile," AIAA-2010-4226, June 2010.

[11]Blair, A. B., Jr., Allen, J. M., and Hernandez, G. "Effect of Tail-Fin Span on the Stability and Control Characteristics of a Canard Controlled Missile at Supersonic Speeds," NASA TP 2157, June 1983.

[12]Beresh, S.J., Smith, J.A., Henfling, J.F., Grasser, T. W., and Spillers, R.W., "Interaction of a Fin Trailing Vortex with a Downstream Control Surface," *Journal of Spacecraft and Rockets*, Vol. 46, No. 2, March–April 2009, pp. 318-328.

[13]Allen, J. M., Shaw, D. S., and Sawyer, W. C., "Analysis of Selected Data From The Triservice Missile Data Base," AIAA 89-0478, Jan. 1989.

[14]Allen, J. M., The Triservice Missile Database, NASA/TM-2002-211653, June 2002.

[15]Allen, J. M., Parametric Fin-Body and Fin-Plate Database for a Series of 12 Missile Fins, NASA/TM-2001-210652, Jan. 2001.

[16]Aftosmis, M.J., Melton, J.E., and Berger, M.J., "Adaptive Cartesian Mesh Generation." Chapter 22 in Handbook of Grid Generation, Thompson, J, Weatherhill, N., and Soni, B. eds. CRC Press 1998.